A

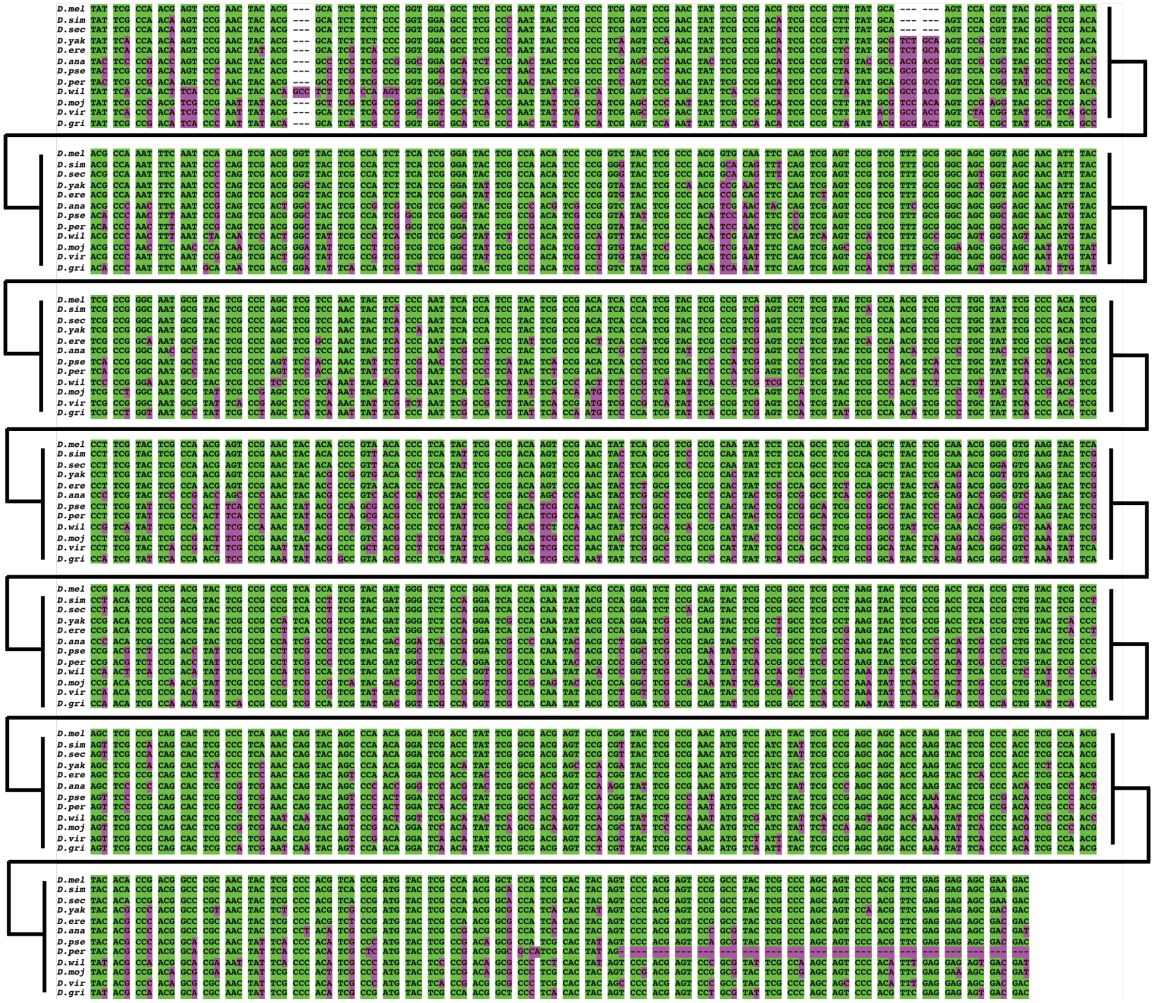

B

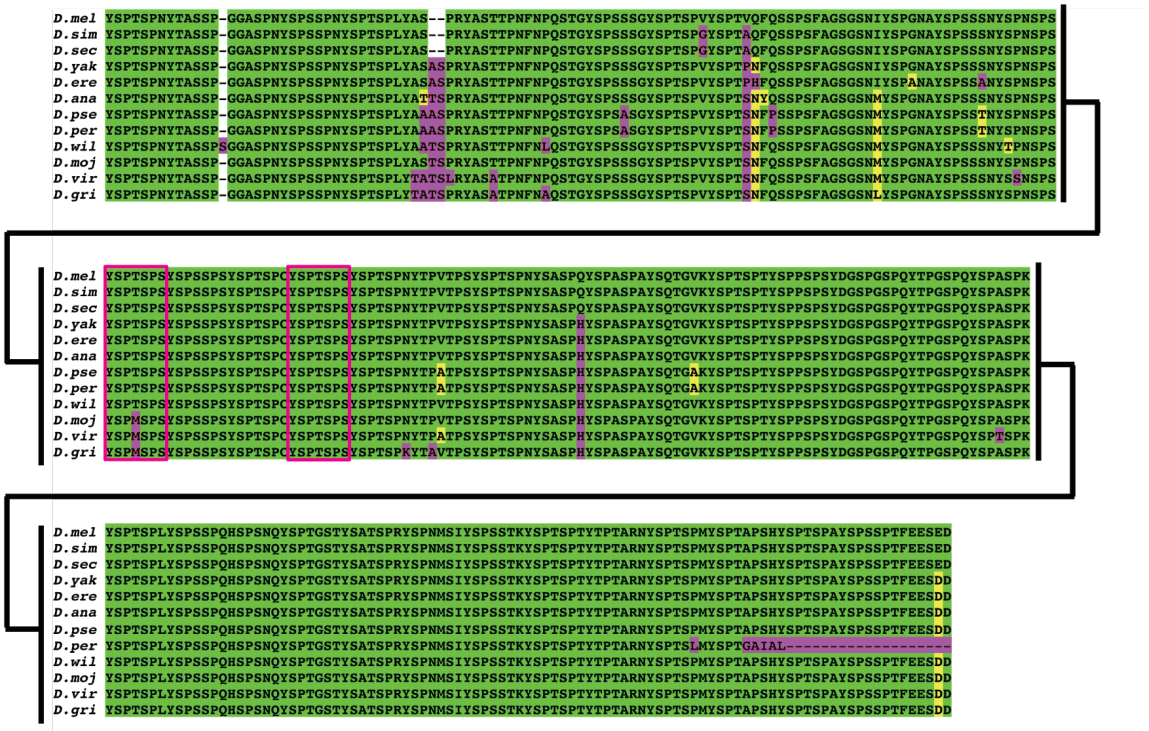

Figure S1. Sequence alignments of the CTDs of *Drosophila*, related to Figure 1B.

(A) Nucleotide sequence alignment of the CTDs from 12 *Drosophila* species. The colors identify nucleotides that are identical (green) or different (magenta) compared with *D. melanogaster*.

(B) Amino acid sequence alignment of the CTDs from 12 *Drosophila* species. The colors identify amino acids that are identical (green), similar (yellow) or dissimilar (magenta) compared with *D. melanogaster*. Pink boxes highlight the only two consensus heptads in the CTD of *D. melanogaster*.

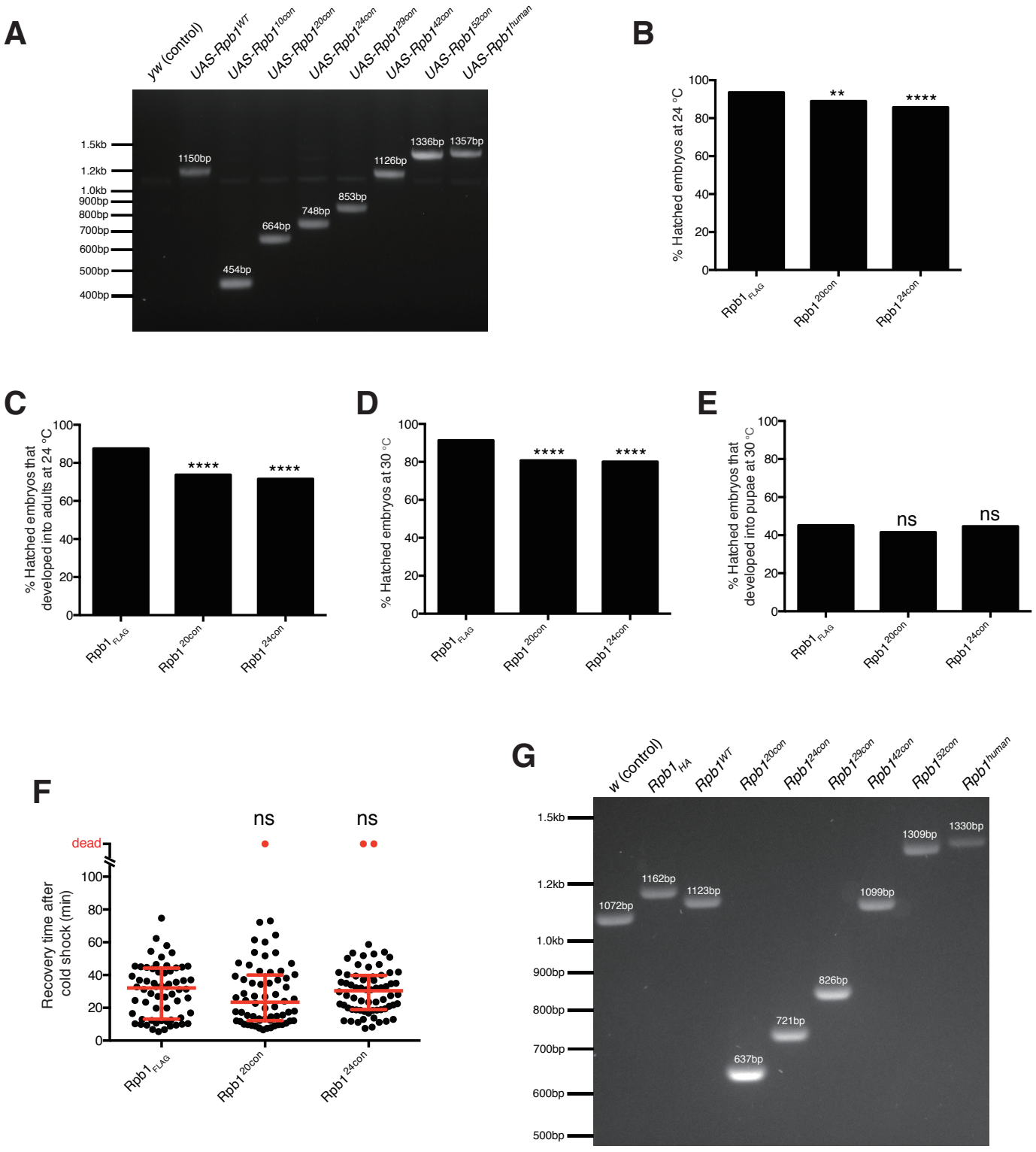
A
yw (control)
UAS-Rpb1WT
UAS-Rpb110con
UAS-Rpb120con
UAS-Rpb124con
UAS-Rpb129con
UAS-Rpb142con
UAS-Rpb152con
UAS-Rpb1human
1.5kb
1.2kb
1.0kb
900bp
800bp
700bp
600bp
500bp
400bp
1150bp
454bp
664bp
748bp
853bp
1126bp
1336bp
1357bp
B
% Hatched embryos at 24 °C
**
****
Rpb1FLAG
Rpb120con
Rpb124con
C
% Hatched embryos that developed into adults at 24 °C
****
****
D
% Hatched embryos at 30 °C
****
****
E
% Hatched embryos that developed into pupae at 30 °C
ns
ns
F
dead
ns
ns
Recovery time after cold shock (min)
G
w (control)
Rpb1HA
Rpb1WT
Rpb120con
Rpb124con
Rpb129con
Rpb142con
Rpb152con
Rpb1human
1072bp
1162bp
1123bp
637bp
721bp
826bp
1099bp
1309bp
1330bp

Figure S2. PCR validation of fly lines and additional physiological parameters of selected Rpb1 mutants, related to Figure 3.

(A) PCR validation of various fly lines carrying *UAS-Rpb1* transgenes. One primer was specific to *UAS-Rpb1* insertion and the other hybridized to the body of *Rpb1*.

(B to F) Replacing the endogenous Rpb1 with either $Rpb1^{20con}$ or $Rpb1^{24con}$ using CRISPR-Cas9 produces healthy homozygous flies. (B) Hatch rates of embryos at 24°C, measured 36h after egg deposition, n>350 for each genotype. (C) Percentages of hatched embryos that developed into adults when raised at 24°C, n>300 for each genotype. (D) Hatch rates of embryos at 30°C, measured 36h after egg deposition, n>350 for each genotype. (E) Percentages of hatched embryos that developed into pupae when raised at 30°C, n>400 for each genotype. (F) Quantification of recovery time after 14h of cold shock on ice, n=64 for $Rpb1_{FLAG}$; n=64 for $Rpb1^{20con}$; n=68 for $Rpb1^{24con}$ (equal numbers of male and female adults were assayed). Dots represent individual adults. Red bars show the medians and interquartile ranges.

(G) PCR validation of hemizygotic males with the modified endogenous Rpb1 locus using primers flanking the CTD. A male fly with unmodified Rpb1 locus [*w*(control)] provides the PCR product of the unmodified locus. Changes in the sizes of the PCR products reflect modification of the endogenous Rpb1 locus.

Two-sided chi-squared tests were used for (B) to (E). Mann–Whitney *U* tests were used for (F). ns: not significant ($p>0.05$), $*p < 0.05$, $**p < 0.01$, $***p < 0.001$ or $****p < 0.0001$ values were considered statistically significant from $Rpb1_{FLAG}$.

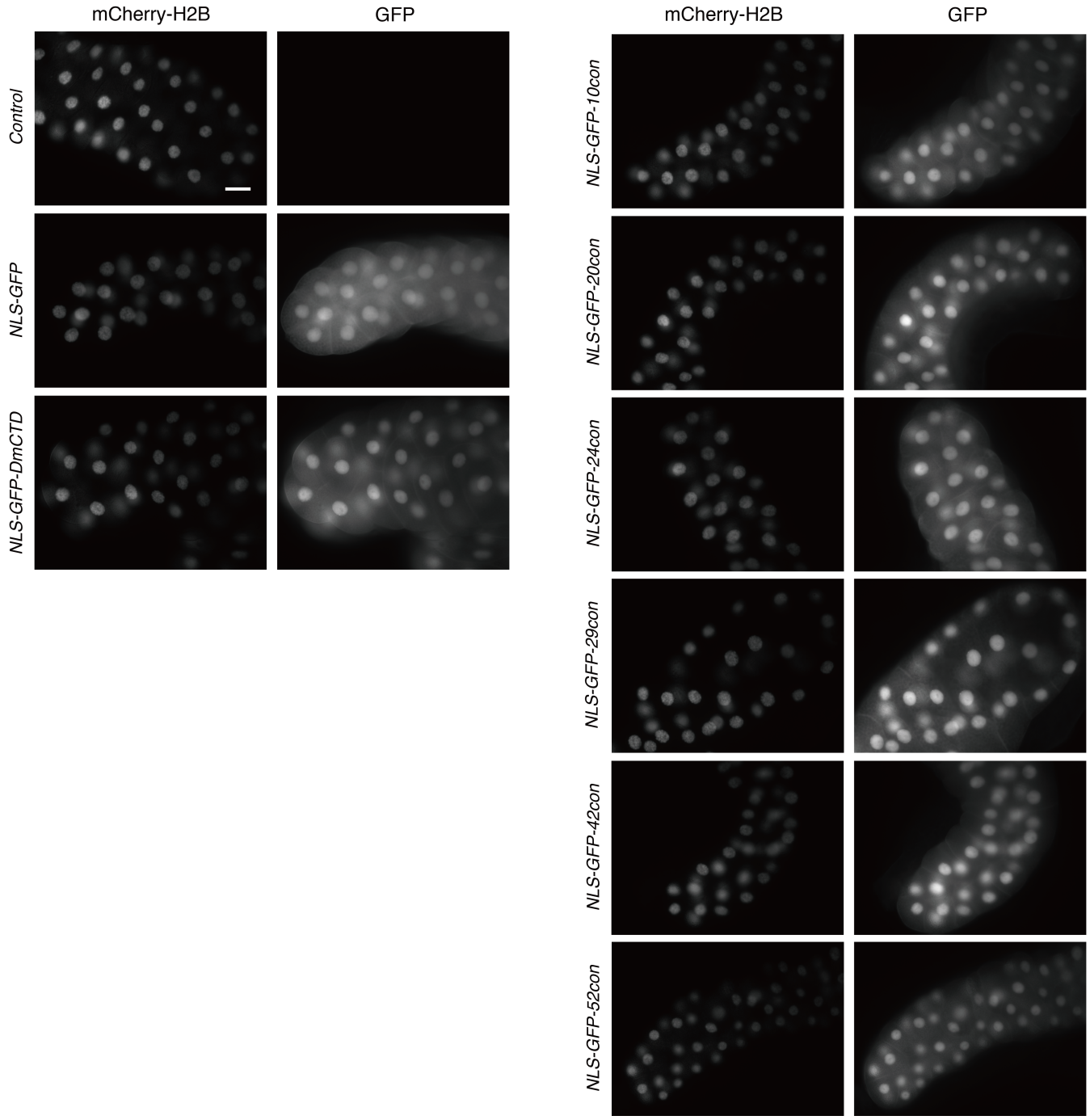

Figure S3. Fluorescence detection of NLS-GFP derivatives in the nuclei of salivary glands, related to Figure 4 and Figure 5. Expression was driven by *Sgs3-GAL4*. Scale bar represents 50 μm.

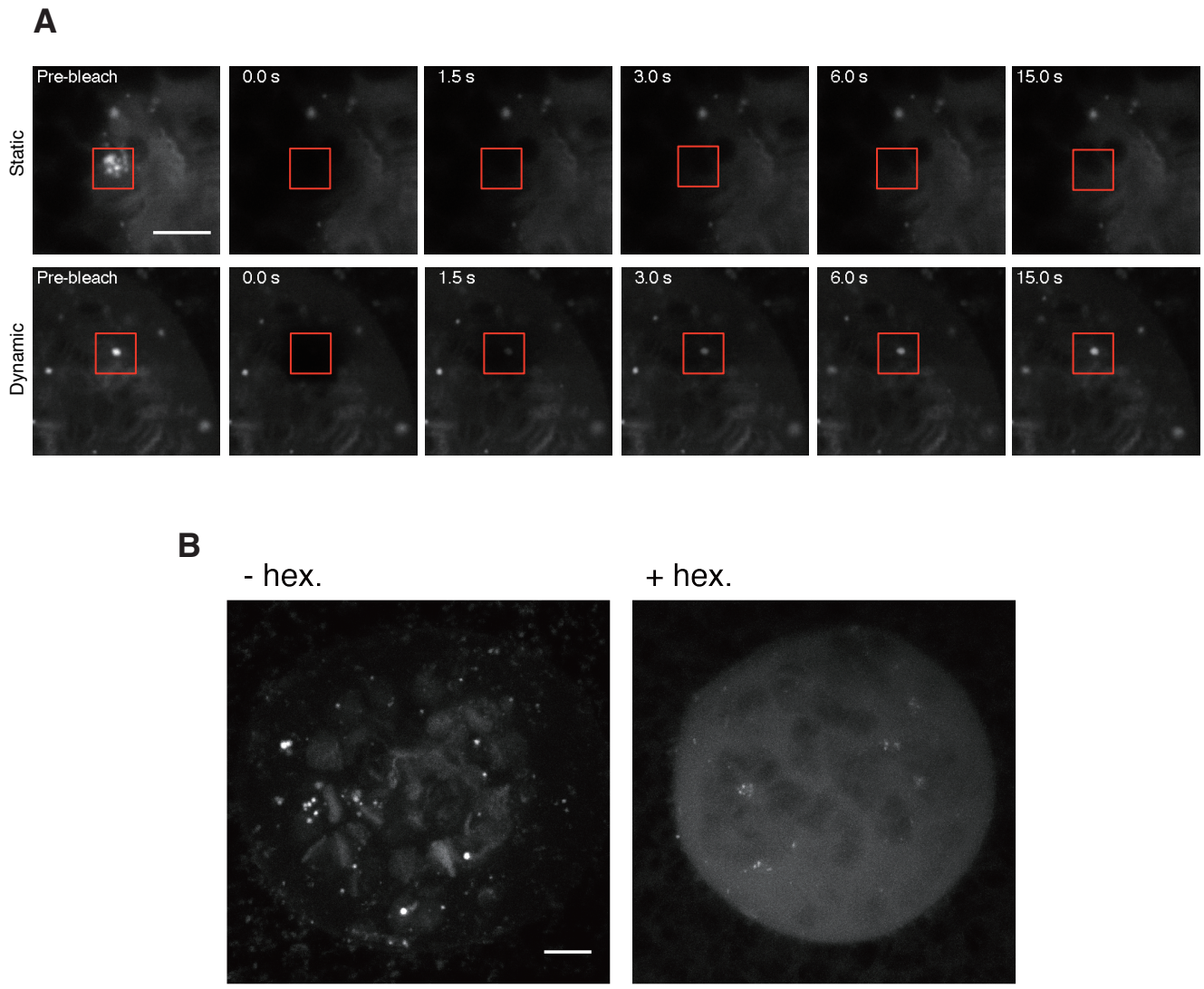

Figure S4. GFP-DmCTD forms static and dynamic foci, part of which is sensitive to 1,6-hexanediol, related to Figure 4.

(A) FRAP analysis reveals that GFP-DmCTD containing foci can be static (upper) or dynamic (lower).

(B) Treatment with 1% 1,6-hexanediol dissolved a subset of GFP-DmCTD foci. Maximum intensity projections of entire Z stacks. The diffuse fluorescence detected after 1,6-hexanediol treatment is due to the release of GFP-DmCTD from the chromosomes.

Both scale bars represent 5 μm.

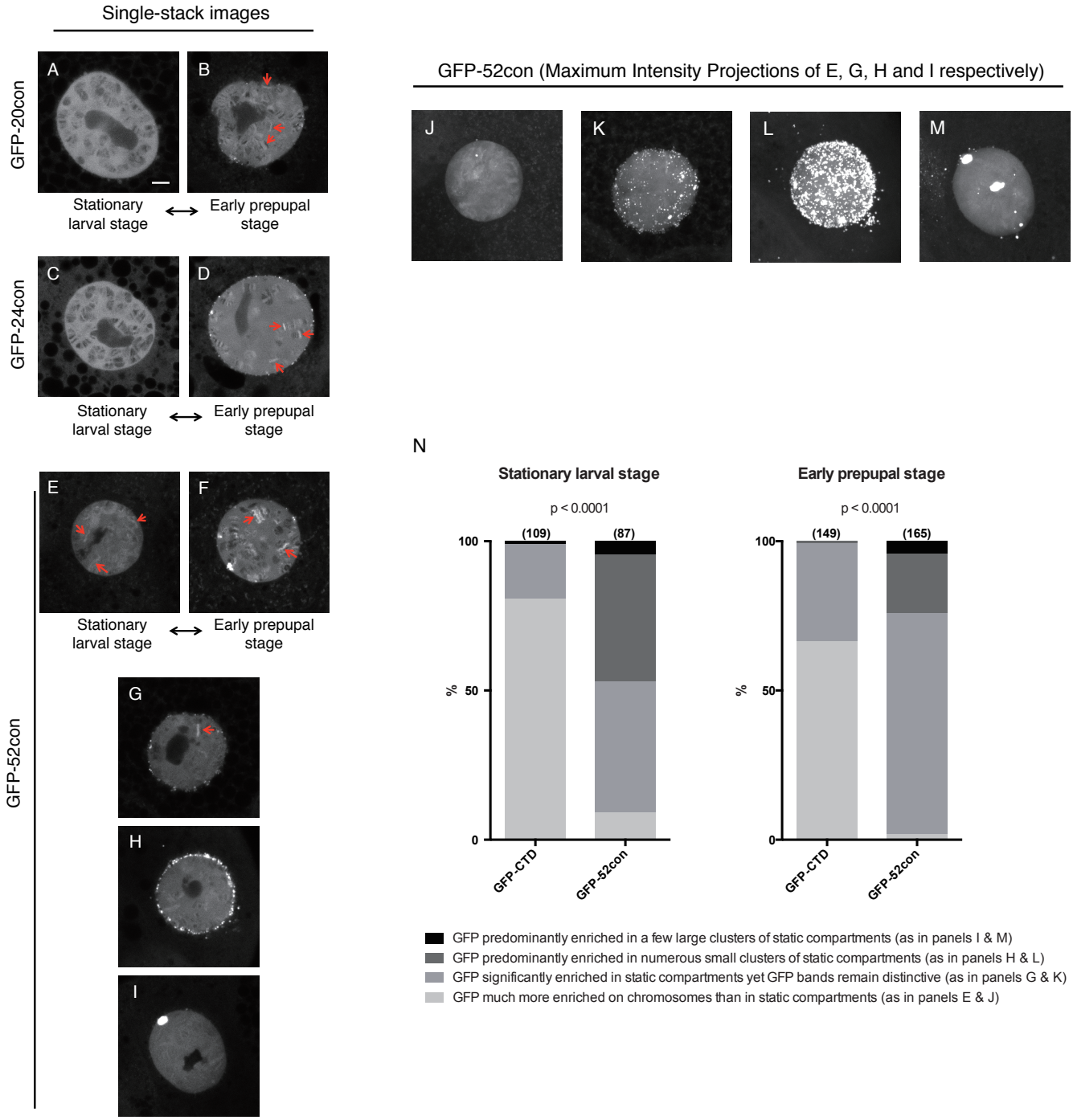
Single-stack images
GFP-20con
A
B
Stationary larval stage
Early prepupal stage
GFP-24con
C
D
Stationary larval stage
Early prepupal stage
GFP-52con
E
F
Stationary larval stage
Early prepupal stage
G
H
I
GFP-52con (Maximum Intensity Projections of E, G, H and I respectively)
J
K
L
M
N
Stationary larval stage
p < 0.0001
(109)
(87)
100
50
0
%
GFP-CTD
GFP-52con
Early prepupal stage
p < 0.0001
(149)
(165)
100
50
0
%
GFP-CTD
GFP-52con
GFP predominantly enriched in a few large clusters of static compartments (as in panels I & M)
GFP predominantly enriched in numerous small clusters of static compartments (as in panels H & L)
GFP significantly enriched in static compartments yet GFP bands remain distinctive (as in panels G & K)
GFP much more enriched on chromosomes than in static compartments (as in panels E & J)

Figure S5. Varying the CTD sequence composition alters its distribution in the nucleus, related to Figure 5.

(A to I) Single-stack confocal images of nuclei in live salivary glands expressing NLS-GFP-20con (A and B), NLS-GFP-24con (C and D) and NLS-GFP-52con (E to I). A, C and E were collected from the stationary larval stage whereas B, D and F were collected from the early prepupal stage. Examples depicted in G, H and I can be observed in both stages. Scale bar represents 5 μm. Red arrows demarcate examples of puffs that show enrichment over the nucleoplasm.

(J to M) Maximum intensity projections of the same nuclei shown in E, G, H and I, respectively.

(N) GFP-52con cells are more prone to partition in static compartments. Sample sizes are indicated in parentheses. Darker shades of gray indicate that more CTD associates with static compartments than with chromosomes. $p<0.0001$, two-sided chi-squared tests.